Research Square

Preprints are preliminary reports that have not undergone peer review.
They should not be considered conclusive, used to inform clinical practice,
or referenced by the media as validated information.

Hydrogen as a Molecular Probe for Nanopore Structure Characterization

Nicholas J Corrente
Rutgers University
Evan Schley
Rutgers University
Sebastian Stock
Montanuniversität Leoben
Oskar Paris
Montanuniversität Leoben
Alexander V Neimark
aneimark@rutgers.edu

Rutgers University

Research Article

Keywords: pore structure characterization, hydrogen adsorption, hydrogen storage, isotope separations, nanoporous carbons, quantum corrections, density functional theory

Posted Date: August 10th, 2026

DOI: https://doi.org/10.21203/rs.3.rs-10580927/v1

License: This work is licensed under a Creative Commons Attribution 4.0 International License.
Read Full License

Additional Declarations: No competing interests reported.

Hydrogen as a Molecular Probe for Nanopore Structure Characterization

Nicholas J Corrente[1], Evan Schley[1], Sebastian Stock[2], Oskar Paris[2], Alexander V Neimark[1,*]

[1] Department of Chemical and Biochemical Engineering, Rutgers University, USA
2 Department Physics, Montanuniversität, Leoben, Franz-Josef-Straße 18, 8700, Leoben, Austria

Email: aneimark@rutgers.edu; Web: http://neimark.rutgers.edu/

Abstract

The design of advanced adsorbents for hydrogen storage and isotope separation requires a reliable methodology for pore-structure characterization. Due to its smallest size and relatively weak adsorption strength, hydrogen preferentially adsorbs in the smallest ultramicropores, which are insufficiently resolved using standard nitrogen adsorption measurements. Here, we demonstrate, using a representative example of ACC-ILL microporous carbon, the advantages of employing hydrogen as a molecular probe for adsorption characterization. The kernels of reference H_2 and D_2 isotherms at 77.4 K in cylindrical carbon pores ranging from 0.35 to 20 nm in diameter are generated with a classical density functional theory (DFT), which accounts for the fluid-solid interactions via statistical associating fluid theory (SAFT) with quantum-corrected Mie potentials (SAFT-VRQ Mie). We found that the isotope-specific differences in adsorption behavior are consistently captured by this quantum-corrected DFT model. The constructed kernels are used to derive the pore-size distributions from the experimental H_2 and D_2 isotherms. Furthermore, we show that the experimental D_2 isotherm can be predicted by convolving the pore-size distribution determined from the experimental H_2 isotherm with the D_2 adsorption kernel. Reliable prediction of D_2 adsorption behavior from relatively inexpensive H_2 experiments greatly expands the practicality of nanoporous material screening for isotope separation applications, where distinguishing candidate materials often depends on subtle differences in confinement behavior that are costly to measure directly. The proposed H_2 adsorption methodology is recommended for testing nanoporous carbons for hydrogen-based applications.

Key words: pore structure characterization, hydrogen adsorption, hydrogen storage, isotope separations, nanoporous carbons, quantum corrections, density functional theory.

Introduction

Hydrogen plays a central role in the emerging clean-energy economy. Beyond its role as a fuel, it is essential to isotopic separation processes that underpin technologies such as medical imaging and nuclear fusion.[1-3] Hydrogen fuel cells offer a compelling route to reducing air pollution and lowering dependence on fossil fuels, yet their broader deployment is limited by unresolved challenges in hydrogen storage.[4] Progress in fuel cell technology, therefore, depends on identifying and optimizing highly porous materials capable of storing hydrogen efficiently. Separating hydrogen from its heavier isotopes is also essential for applications in medical diagnostics and nuclear technology.[2, 3] Established separation methods, including cryogenic distillation and chemical exchange processes, remain costly and energy-intensive, pointing to the need for more efficient, materials-based alternatives.[5, 6]

Nanoporous materials, including activated carbons and metal-organic frameworks (MOFs), have emerged as leading candidates for hydrogen storage and isotope separation because of their large surface areas and pore volumes.[7, 8] Nanoporous carbons, with their broad pore size distributions (PSD) and large accessible volumes, frequently achieve better volumetric hydrogen uptake than MOFs with comparable gravimetric performance.[9] Both classes of materials can be further enhanced through chemical treatments designed to increase the fraction of surface area available for hydrogen adsorption.[10] Fully capitalizing on these materials, however, requires a precise, mechanistic understanding of how hydrogen and deuterium behave once confined within nanopores.

This understanding, in turn, depends on the ability to accurately characterize nanopore structure, since pore geometry directly governs adsorption thermodynamics. Standard adsorption-based characterization relies on probe molecules such as nitrogen at 77 K, argon at 87 K, and carbon dioxide at 273 K.[11] These conventional probes are limited in hydrogen adsorption characterization, as their molecular size prevents them from penetrating the tiniest ultramicropores accessible to hydrogen and deuterium. Using hydrogen as a probe molecule directly addresses this shortcoming, enabling exploration of ultramicropores while providing information on the specific adsorbent-hydrogen interactions most relevant to storage applications.

This rationale is supported by a recent neutron-scattering and adsorption study,[8] which found that hydrogen and deuterium uptake in nanoporous carbons depends strongly on the degree of confinement, with the most pronounced densification occurring in ultramicropores only slightly larger than the hydrogen molecule (around 0.35 - 0.45 nm), a size range that nitrogen and argon cannot resolve well. It was found that deuterium adsorbs more strongly than hydrogen, a difference attributed to their distinct zero-point energies, suggesting that quantum effects cannot be ignored under these conditions. These findings point to the promise of hydrogen as a structural probe, motivating the development of pore-size characterization methods based on hydrogen adsorption measurements.

Density functional theory (DFT) methods allow for the generation of a kernel of theoretical adsorption isotherms across a wide range of pore sizes for a chosen adsorbent-adsorbate pair.[11, 12] These theoretical isotherms make it possible to distinguish how adsorption and capillary condensation differ with pore size and shape.[13-15] Two DFT variants in particular, non-local DFT (NLDFT) and quenched solid DFT (QSDFT),[12, 13] are included in the software of

commercial adsorption instruments and are now recommended as preferred standard methods.[11] These DFT-based kernel methods have also been paired with percolation network models that capture additional real-world complications such a pore blocking, cavitation, metastability, and pore network connectivity.[12, 16-18]

Care must be taken when applying these DFT methods to hydrogen, since its low mass makes quantum effects unavoidable at cryogenic temperatures. A lighter molecule such as hydrogen adsorbs less strongly to a surface than classical mechanics alone would predict; deuterium, being heavier, has a correspondingly lower zero-point energy and adsorbs more readily, an effect that becomes noticeable in the narrowest ultramicropores.[8] Ordinary classical potentials cannot reproduce this isotope-dependent contrast, since they assign hydrogen and deuterium nearly identical interaction energies, necessitating quantum corrections.[8, 19, 20] The most developed method for this purpose is the statistical associating fluid theory (SAFT) built around quantum-corrected Mie potentials with variable-range attraction and elecrostatics (SAFT-VRQ Mie),[19, 20] which modifies the standard Mie potential[21] with a Feynman-Hibbs correction term[22] linking the interaction energy to particle mass and temperature. The SAFT-VRQ Mie model accurately reproduced the surface tensions of hydrogen and deuterium at temperatures above saturation.[23]

Building on this framework, this study uses a quantum-corrected classical DFT to generate the kernels of reference H_2 and D_2 isotherms at 77.4 K for cylindrical carbon pores ranging from 0.35 to 20 nm in diameter. These kernels are then used to determine the PSDs from experimental H_2 and D_2 isotherms measured on the nanoporous carbon ACC-ILL taken as a case-study example.[8, 24] The advantage of using hydrogen as a probe molecule is demonstrated by comparing the PSDs against the PSD obtained using the conventional NLDFT method applied to nitrogen isotherms on the same sample. Finally, the predictive power of the quantum-corrected DFT approach is tested by using the H_2-derived PSD to predict the corresponding experimental D_2 isotherm. This capability has an important practical value given how costly and limited deuterium measurements typically are.

Methods

Calculations are done using the SAFT-VRQ Mie model, which is designed to account for the quantum effects of hydrogen and similar gases at low temperatures. The modified Mie potential is presented in the following form, [19]

$$u_{ij}(r_{ij}) = C(\lambda_{r,ij}, \lambda_{a,ij})\epsilon_{ij}\left[\frac{\sigma_{ij}^{\lambda_{r,ij}}}{r_{ij}^{\lambda_{r,ij}}} - \frac{\sigma_{ij}^{\lambda_{a,ij}}}{r_{ij}^{\lambda_{a,ij}}} + \frac{\beta\hbar^2}{24m_{ij}}\left(Q_1(\lambda_{r,ij})\frac{\sigma_{ij}^{\lambda_{r,ij}}}{r_{ij}^{\lambda_{r,ij}+2}} - Q_1(\lambda_{a,ij})\frac{\sigma_{ij}^{\lambda_{a,ij}}}{r_{ij}^{\lambda_{a,ij}+2}}\right)\right] \quad (1)$$

where λ_a and λ_r are the attractive and repulsive exponents, respectively; ε represents potential well depth; σ is the distance at which the interparticle potential becomes zero; $C(\lambda_r, \lambda_a) = \left(\frac{\lambda_r}{\lambda_r - \lambda_a}\right)\left(\frac{\lambda_r}{\lambda_a}\right)^{\frac{\lambda_a}{\lambda_r - \lambda_a}}$ is a normalization constant that depends on the Mie exponents, $Q_1(\lambda_i) = \lambda_i(\lambda_i - 1);\ \beta = 1/(k_B T)$ is the inverse temperature, where k_B is the Boltzmann

constant; $\hbar$ is the reduced Planck constant; and $m_{ij} = \frac{m_i m_j}{m_i + m_j}$ is the reduced mass of particles i and j. Mie potentials do not have fixed attractive and repulsive exponents, allowing them to be tailored more effectively to model specific molecules. The Feynman-Hibbs correction is added to account for temperature and reduced mass, which are non-negligible for molecules as small as hydrogen. The Mie potential parameters are listed in Table 1.

Table 1: Mie potential parameters for use with Feynman-Hibbs correction [26]

Substance	$\boldsymbol{\sigma}$/Å	$(\boldsymbol{\varepsilon}/\boldsymbol{k_B})/\boldsymbol{K}$	$\boldsymbol{\lambda_r}$	$\boldsymbol{\lambda_a}$
Hydrogen	3.0243	26.706	9	6
Deuterium	3.0203	30.273	10	6

Solid-fluid interactions are modeled by the Steele 10-4-3 potential adapted for cylindrical geometry, shown in Eq. (2), [25, 26]

$$V_{C,10-4-3}(r,R) = 2\pi\rho_s \Delta\sigma^2\epsilon\left[\psi_6(r,R,\sigma) - \psi_3(r,R,\sigma) - \frac{\sigma}{\Delta}\varphi_3(r,R+\alpha\Delta,\sigma)\right]. \quad (2)$$

Here r is the radial position of the fluid molecule from the pore center, R is the pore radius, ρ_s is the volume density of the adsorbent, Δ is the spacing between basal planes,

$$\varphi_n(r,R,\sigma) = \frac{4\sqrt{\pi}}{2n-3}\frac{\Gamma\left(n,\ -,\ \frac{1}{2}\right)}{\Gamma(n)}\left(\frac{\sigma}{R}\right)^{2n-3}\left[1-\left(\frac{r}{R}\right)^2\right]^{3-2n} \times F\left(\frac{3-2n}{2},\frac{5-2n}{2};1;\left(\frac{r}{R}\right)^2\right), \quad (3)$$

$$\psi_n(r,R,\sigma) = 4\sqrt{\pi}\frac{\Gamma\left(n,-,\frac{1}{2}\right)}{\Gamma(n)}\left(\frac{\sigma}{R}\right)^{2n-2}\left[1-\left(\frac{r}{R}\right)^2\right]^{2-2n} \times F\left(\frac{3-2n}{2},\frac{3-2n}{2};1;\left(\frac{r}{R}\right)^2\right), \quad (4)$$

Γ is the Gamma function, and F is the hypergeometric function. The cylindrical modification accounts for curvature effects, with ψ_6 and ψ_3 representing summations of pairwise interactions integrated over the first layer of carbon atoms forming the pore wall (ψ_6 represents the attractive van der Waals forces and ψ_3 the repulsive interactions). φ_3 accounts for long-range dispersion interactions from deeper atomic layers, and α accounts for the effective position of the solid's outer edge.

We calculated the kernel of theoretical adsorption isotherms, $N_{theor}(p/p^0, W)$, in carbon cylindrical pores in the range of pore diameters, 0.35 nm $< W <$ 20 nm using the open-source FeOs software.[27] The pore size distribution, $f(W)$, is determined by deconvolution of the generalized adsorption isotherm equation,

$$N_{exp}(p/p^0) = \int_{W_{min}}^{W_{max}} N_{theor}(p/p^0, W) f(W) dW, \quad (5)$$

which presents the experimental isotherm, $N_{exp}(p/p^0)$, as a weighted sum of reference isotherms.[11] Eq. (5) allows for the determination of PSDs by correlating simulated adsorption kernels with experimentally measured adsorption data. It should be noted that the deconvolution procedure is an inverse problem that requires numerical regularization techniques to yield physically meaningful solutions.[28]

The methodology is demonstrated using the PSD calculations for the nanoporous carbon ACC-ILL[8, 24]. This adsorbent is derived from viscose rayon cloth via $ZnCl_2$/NH_4Cl impregnation, carbonization, and CO_2 activation. It has the nitrogen adsorption measured BET surface area of 1200 m^2/g and pore volume of 0.5 cm^3/g, with a mean pore width of ~0.6 - 0.7 nm with >90% porosity in its micropores. Kostoglou et al.[24] report fully reversible hydrogen cryo-adsorption on this material, with capacities of 1.68 wt% at 77 K and 1 bar. The cloth morphology also yields a mechanically flexible, binder-free sorbent architecture, making ACC-ILL a practical hydrogen adsorbent for integration into storage systems. Adsorption measurements on ACC-ILL sample were performed on an Autosorb iQ3 (Anton Paar QuantaTec),[8] and the resulting N_2, H_2, and D_2 isotherms were used to compare pore size distributions from our H_2/D_2 adsorption kernels, N_{theor,H_2} and N_{theor,D_2}, against those obtained from a conventional N_2 NLDFT kernel. Also, we demonstrate that the experimental D_2 isotherm can be predicted from the measured H_2 isotherm. In doing so, we first determine the PSD of the sample from the experimental H_2 isotherm and the theoretical H_2 kernel, $f_{H_2}(W)$, and then convolute the theoretical D_2 kernel with this PSD:

$$N_{exp,D_2}(p/p^0) = \int_{W_{min}}^{W_{max}} N_{theor,D_2}(p/p^0, W) f_{H_2}(W) dW. \quad (6)$$

The calculated D_2 isotherm is found in good agreement with the experimentally measured isotherm.

Results & Discussion

Figure 1 shows characteristic theoretical hydrogen and deuterium isotherms separately in the ultramicropores (0.3575 - 0.7 nm) and supermicropores (0.7 – 2 nm) in the range of pressures from $p/p_0 = 10^{-9}$ to 1, where p_0 is the saturation pressure of the adsorbate. Adsorption is notably stronger in ultramicropores, and deuterium consistently exhibits slightly higher adsorption than hydrogen, as seen in Fig. 2. In the narrowest pores, adsorption is dominated by a single, tightly packed layer of molecules. The close proximity of the pore walls amplifies intermolecular interactions. As pore size increases, the adsorbate density gradually decreases because the adsorbate cannot stabilize a second layer. In larger pores, where the walls are too far apart for significant cross-pore interactions, adsorption proceeds weakly, directly on the pore surface.

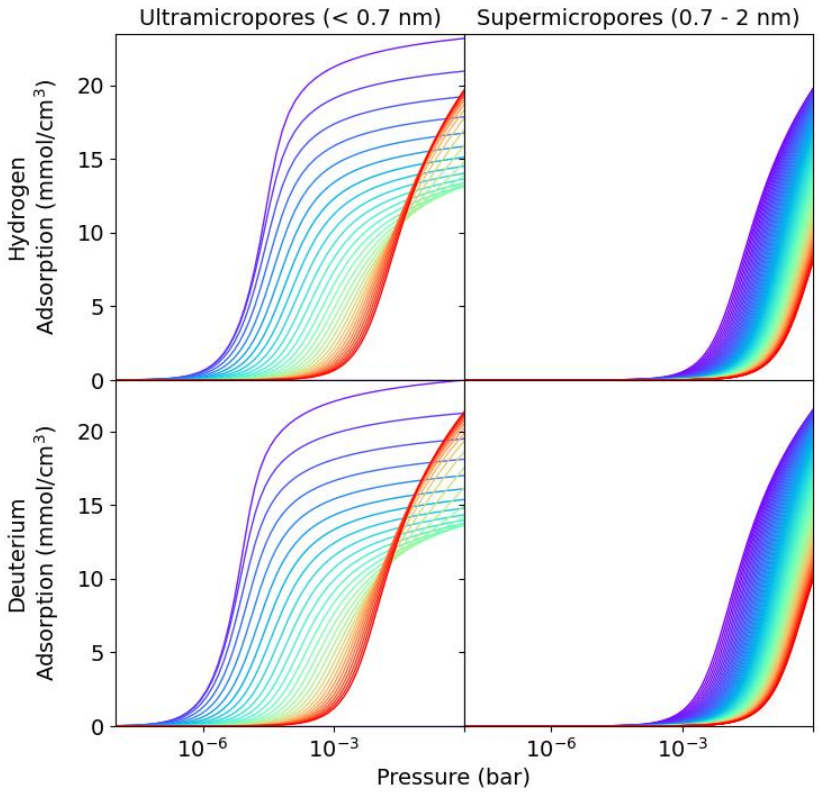


Figure 1: Kernels of hydrogen (top) and deuterium (bottom) ultramicropores (left) and supermicropores (right).

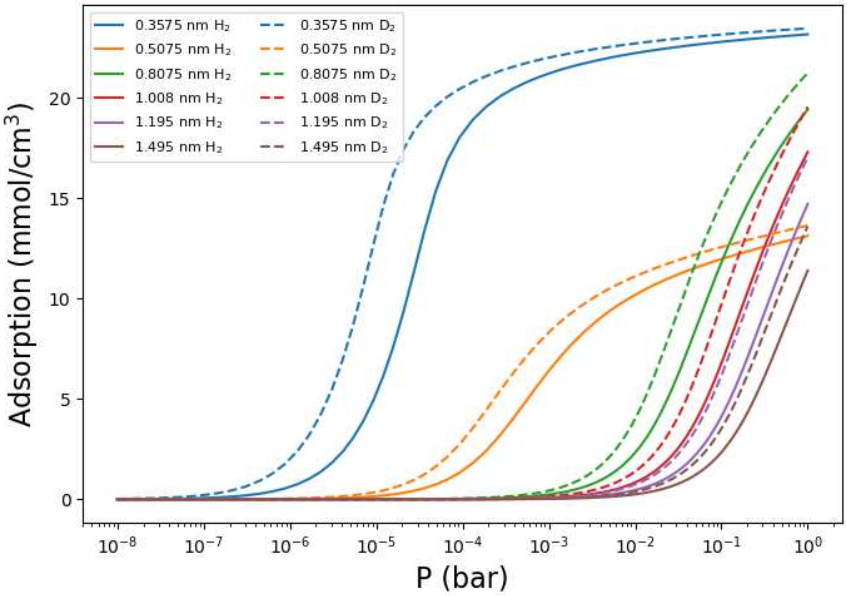


Figure 2: Comparison of hydrogen and deuterium isotherms in micropores of different sizes.

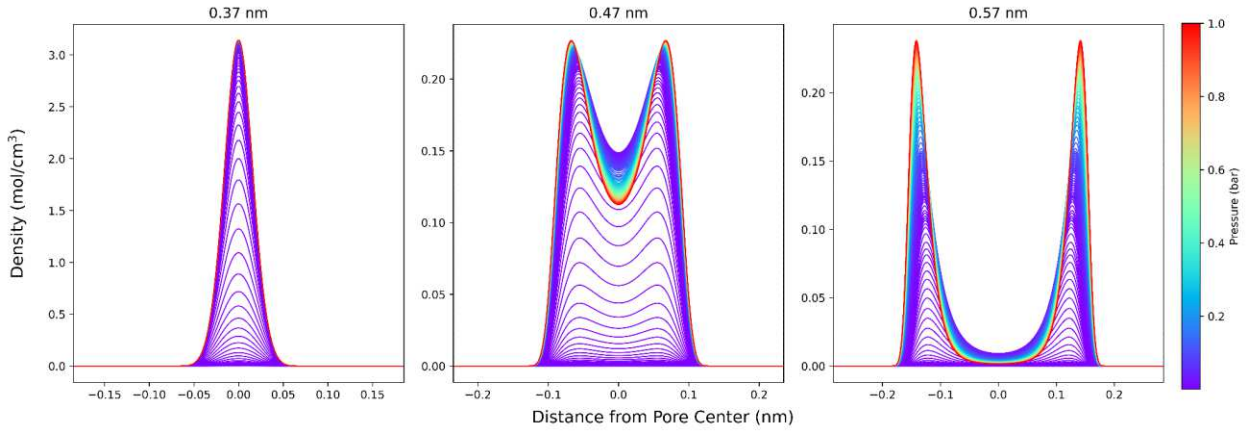


Figure 3: Evolution of the density profiles of hydrogen in cylindrical pores with increasing gas pressure.

Figure 3 presents radial density profiles of hydrogen in simulated cylindrical carbon pores of widths 0.37, 0.47, and 0.57 nm, illustrating how adsorption structure evolves as the pore size increases. In the narrowest pore (left), there is only room for a dense single file of molecules, resulting in one sharp density peak at the pore center growing as the pressure increases. At 0.47 nm, the pore is large enough to disrupt axial ordering but too small to accommodate two molecules within its cross-section, producing a frustrated zigzag configuration. At low pressures, adsorbed molecules freely move between the pore that results in almost uniform radial density distribution, while as the pressure increases, the density shifts toward the pore walls as an interplay of fluid-solid and fluid-fluid interactions favors off-center near-surface positions. In the 0.57 nm pore, adsorption density transitions to the classical wall-layering behavior, with density maxima near the pore walls and the comparatively depleted pore center. Together, these profiles demonstrate the progression with the increase of the pore size from single-file confinement to packing frustration to monolayers to single-layer surface adsorption.[29]

Figure 4 shows differential PSDs derived from the H_2, D_2, and N_2 experimental isotherms on ACC-ILL activated carbon using the calculated hydrogen and deuterium kernels and a nitrogen NLDFT kernel generated on cylindrical carbon pores.[12]The PSDs were obtained by the deconvolution of Eq. 5 using a non-negative least squares optimization method with Tikhonov regularization.[30] All three adsorbates yield PSDs with a comparable population of pores in the 0.5-1.5 nm ultra- and supermicropore range, consistent with the microporous structure reported for ACC-ILL.[8, 24]However, close inspection of the individual peaks within this range reveals substantial differences in resolution between the three probes.

Both H_2 and D_2 resolve distinct ultramicropore populations between 0.4-0.7 nm, which are the main contributors to adsorption together with smaller supermicropores, from 0.7-1.5 nm. Notably, the PSDs for H_2 and D_2 are very similar, with minor deviations that insignificantly affect the isotherm fitting. In contrast, N_2 exhibits a single sharp peak in the ultramicropore range at ~0.6 nm, and an extended distribution of larger supermicropores and smaller mesopores. This enhanced resolution in the H_2 and D_2 PSDs is a direct consequence of their smaller kinetic diameters relative to N_2, which allow them to probe smaller pore sizes and to access pore spaces that are inaccessible to larger probes. The practical implication is that PSDs

obtained from N_2 adsorption alone may under-resolve or entirely miss distinct ultramicropore populations that are of particular relevance to hydrogen storage, reinforcing the value of H_2 and D_2 as complementary, higher-resolution structural probes for this pore size regime.

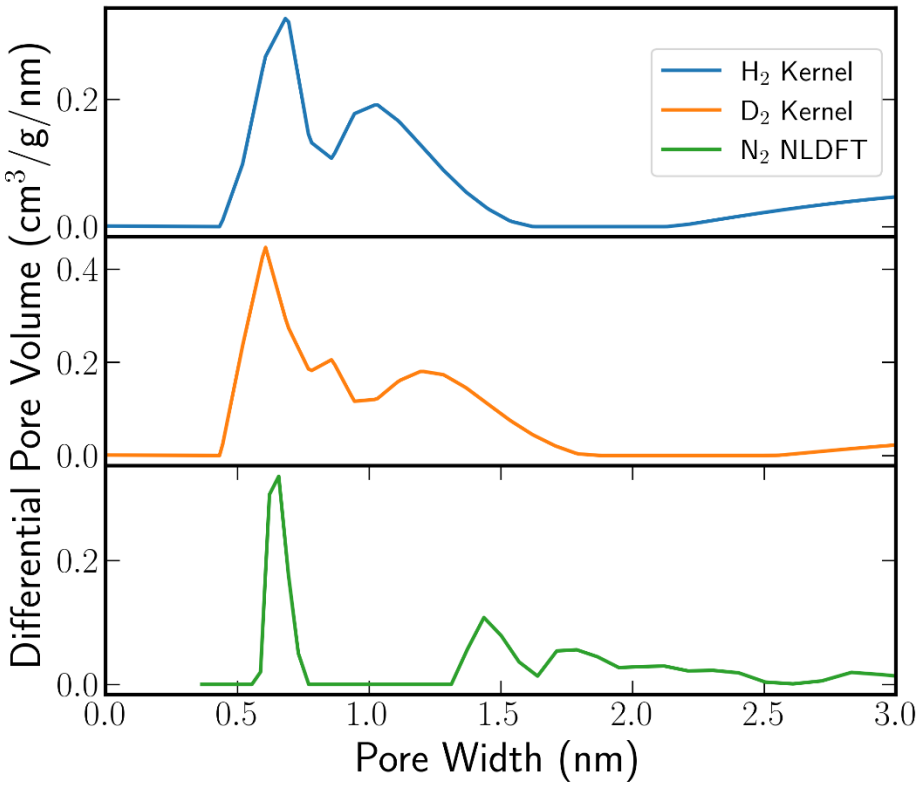


Figure 4: Differential Pore Size Distributions for ACC-ILL sample obtained from fitting the experimental isotherms to the theoretical kernels: H_2 (top), D_2 (center), and N_2 (bottom).

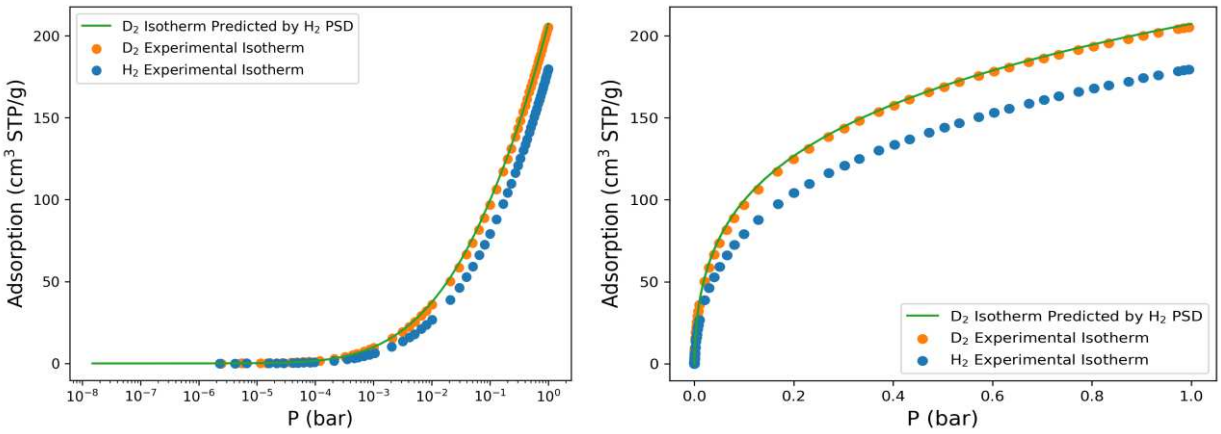


Figure 5: Predicted D_2 experimental isotherm from the PSD determined from the H_2 isotherm in semilog (left) and linear (right) scales.

To demonstrate the advantage of using hydrogen as a molecular probe, we predicted the experimental deuterium isotherm based on the pore size distributions determined independently from the hydrogen isotherm. The predicted D_2 isotherm was obtained by

convolving the H_2-derived PSD, $f_{H2}(w)$, with the theoretical D_2 kernel, N_{theor,D_2}, following the generalized adsorption isotherm relationship introduced in Eq. 6. Figure 5 shows ideal agreement between this prediction and the actual experimental D_2 isotherm across both logarithmic (left) and linear (right) scales, capturing the overall uptake and shape of the isotherm across the full pressure range. This level of agreement is notable given that the H_2 and D_2 kernels differ in their underlying Mie potential parameters and Feynman-Hibbs quantum corrections, meaning the prediction implicitly tests whether the pore structure recovered from one isotope's adsorption behavior is physically transferable to the other. It is worth noting that the use of the N_2-derived PSD underpredicts the experimental D_2 isotherm, see Figure S2. The success of this cross-isotope prediction supports the conclusion that the PSD extracted from the H_2 isotherm reflects the underlying pore geometry of ACC-ILL.

Conclusions

The use of hydrogen as an adsorbate for characterizing nanoporous materials offers distinct advantages over traditional probe molecules. Owing to its small molecular size, hydrogen can access ultramicropores that are not readily accessible to larger adsorbates. This capability enables a more comprehensive assessment of pore structures, particularly at the sub-nanometer scale, and allows for more accurate estimation of adsorption capacity in the pore size range most relevant to hydrogen storage.

This work demonstrates that hydrogen adsorption offers both structural and functional advantages for characterizing nanoporous materials, particularly those dominated by ultramicropores. The pore size distributions obtained from the H_2 and D_2 kernels resolved more pore sizes than the conventional N_2-derived PSD, especially within the 0.4–1 nm range, indicating that hydrogen and deuterium can probe ultramicropore populations that nitrogen cannot access. Materials that selectively adsorb hydrogen in pores too small for nitrogen may exhibit enhanced hydrogen storage capacity or favorable isotopic separation properties that would otherwise go undetected by conventional nitrogen adsorption methods. Thus, hydrogen serves not only as a superior structural probe but also as a means for identifying materials with application-relevant performance.

The ability to predict deuterium adsorption isotherms using the hydrogen-derived pore size distribution is especially significant given the high cost and limited availability of deuterium experiments. Because this prediction relies solely on the H_2-derived PSD, without fitting to the experimental D_2 data, the strong agreement across both linear and logarithmic pressure scales serves as independent validation of both the recovered pore structure and the quantum-corrected DFT framework used to generate the H_2 and D_2 kernels. This result indicates that the isotope-specific differences in adsorption behavior are consistently captured by the model, without requiring separate empirical adjustments for each isotope. Reliable prediction of deuterium adsorption behavior from relatively inexpensive hydrogen experiments greatly expands the practicality of nanoporous material screening for isotope separation applications, where distinguishing candidate materials often depends on subtle differences in confinement behavior that are costly to measure directly.

The constructed kernels are deposited on GitHub and made available to the community to support further development and application of hydrogen-based pore size characterization methods.

References

(1) Broom, D. P.; Webb, C. J.; Fanourgakis, G. S.; Froudakis, G. E.; Trikalitis, P. N.; Hirscher, M. Concepts for improving hydrogen storage in nanoporous materials. *International Journal of Hydrogen Energy* **2019**, *44* (15), 7768-7779. DOI: https://doi.org/10.1016/j.ijhydene.2019.01.224.

(2) De Feyter, H. M.; Behar, K. L.; Corbin, Z. A.; Fulbright, R. K.; Brown, P. B.; McIntyre, S.; Nixon, T. W.; Rothman, D. L.; de Graaf, R. A. Deuterium metabolic imaging (DMI) for MRI-based 3D mapping of metabolism in vivo. *Science advances* **2018**, *4* (8), eaat7314.

(3) Hupin, G.; Quaglioni, S.; Navrátil, P. Ab initio predictions for polarized deuterium-tritium thermonuclear fusion. *Nature communications* **2019**, *10* (1), 351.

(4) Thomas, K. M. Hydrogen adsorption and storage on porous materials. *Catalysis today* **2007**, *120* (3-4), 389-398.

(5) Kim, J. Y.; Oh, H.; Moon, H. R. Hydrogen isotope separation in confined nanospaces: carbons, zeolites, metal–organic frameworks, and covalent organic frameworks. *Advanced Materials* **2019**, *31* (20), 1805293.

(6) Oh, H.; Savchenko, I.; Mavrandonakis, A.; Heine, T.; Hirscher, M. Highly effective hydrogen isotope separation in nanoporous metal–organic frameworks with open metal sites: direct measurement and theoretical analysis. *ACS nano* **2014**, *8* (1), 761-770.

(7) Parashar, S.; Neimark, A. V. Pore Structure Compartmentalization for Advanced Characterization of Metal–Organic Framework Materials. *Journal of Chemical Information and Modeling* **2024**, *64* (8), 3260-3268.

(8) Stock, S.; Corrente, N.; Seyffertitz, M.; Rauscher, M. V.; Zeiler, S.; Kostoglou, N.; Demé, B.; Marks, N. A.; Neimark, A. V.; Paris, O. On the supercritical adsorption of molecular hydrogen and deuterium in microporous carbons. *Carbon* **2025**, 120436.

(9) Juan-Juan, J.; Marco-Lozar, J.; Suárez-García, F.; Cazorla-Amorós, D.; Linares-Solano, A. A comparison of hydrogen storage in activated carbons and a metal–organic framework (MOF-5). *Carbon* **2010**, *48* (10), 2906-2909.

(10) Bénard, P.; Chahine, R.; Chandonia, P.; Cossement, D.; Dorval-Douville, G.; Lafi, L.; Lachance, P.; Paggiaro, R.; Poirier, E. Comparison of hydrogen adsorption on nanoporous materials. *Journal of Alloys and Compounds* **2007**, *446*, 380-384.

(11) Thommes, M.; Kaneko, K.; Neimark, A. V.; Olivier, J. P.; Rodriguez-Reinoso, F.; Rouquerol, J.; Sing, K. S. Physisorption of gases, with special reference to the evaluation of surface area and pore size distribution (IUPAC Technical Report). *Pure and applied chemistry* **2015**, *87* (9-10), 1051-1069.

(12) Landers, J.; Gor, G. Y.; Neimark, A. V. Density functional theory methods for characterization of porous materials. *Colloids and Surfaces A: Physicochemical and Engineering Aspects* **2013**, *437*, 3-32.

(13) Neimark, A. V.; Lin, Y.; Ravikovitch, P. I.; Thommes, M. Quenched solid density functional theory and pore size analysis of micro-mesoporous carbons. *Carbon* **2009**, *47* (7), 1617-1628.
(14) Neimark, A. V.; Ravikovitch, P. I. Capillary condensation in MMS and pore structure characterization. *Microporous and Mesoporous Materials* **2001**, *44*, 697-707.
(15) Ravikovitch, P.; Domhnaill, S. Ó.; Neimark, A. V.; Schüth, F.; Unger, K. Capillary hysteresis in nanopores: theoretical and experimental studies of nitrogen adsorption on MCM-41. *Langmuir* **1995**, *11* (12), 4765-4772.
(16) Cimino, R.; Cychosz, K. A.; Thommes, M.; Neimark, A. V. Experimental and theoretical studies of scanning adsorption–desorption isotherms. *Colloids and Surfaces A: Physicochemical and Engineering Aspects* **2013**, *437*, 76-89.
(17) Söllner, J.; Neimark, A. V.; Thommes, M. Development and Application of an Advanced Percolation Model for Pore Network Characterization by Physical Adsorption. *Langmuir* **2024**, *40* (44), 23146-23168. DOI: 10.1021/acs.langmuir.4c01042.
(18) Söllner, J.; Corrente, N. J.; Parashar, S.; Neimark, A. V.; Thommes, M. Monte Carlo Simulation of Cooperative Condensation in Nanopore
2 Networks. *Langmuir* **2026. In Press**.
(19) Aasen, A.; Hammer, M.; Ervik, Å.; Müller, E. A.; Wilhelmsen, Ø. Equation of state and force fields for Feynman–Hibbs-corrected Mie fluids. I. Application to pure helium, neon, hydrogen, and deuterium. *The Journal of Chemical Physics* **2019**, *151* (6).
(20) Aasen, A.; Hammer, M.; Müller, E. A.; Wilhelmsen, Ø. Equation of state and force fields for Feynman–Hibbs-corrected Mie fluids. II. Application to mixtures of helium, neon, hydrogen, and deuterium. *The Journal of Chemical Physics* **2020**, *152* (7).
(21) Mie, G. Zur kinetischen Theorie der einatomigen Körper. *Annalen der Physik* **1903**, *316* (8), 657-697. DOI: https://doi.org/10.1002/andp.19033160802.
(22) Feynman, R. P.; Hibbs, A. R.; Styer, D. F. *Quantum mechanics and path integrals*; Courier Corporation, 2010.
(23) Hammer, M.; Bauer, G.; Stierle, R.; Gross, J.; Wilhelmsen, Ø. Classical density functional theory for interfacial properties of hydrogen, helium, deuterium, neon, and their mixtures. *The Journal of Chemical Physics* **2023**, *158* (10).
(24) Kostoglou, N.; Koczwara, C.; Prehal, C.; Terziyska, V.; Babic, B.; Matovic, B.; Constantinides, G.; Tampaxis, C.; Charalambopoulou, G.; Steriotis, T. Nanoporous activated carbon cloth as a versatile material for hydrogen adsorption, selective gas separation and electrochemical energy storage. *Nano Energy* **2017**, *40*, 49-64.
(25) Siderius, D. W.; Gelb, L. D. Extension of the Steele 10-4-3 potential for adsorption calculations in cylindrical, spherical, and other pore geometries. *The Journal of chemical physics* **2011**, *135* (8).
(26) Steele, W. A. The physical interaction of gases with crystalline solids: I. Gas-solid energies and properties of isolated adsorbed atoms. *Surface Science* **1973**, *36* (1), 317-352.
(27) Rehner, P.; Bauer, G.; Gross, J. Feos: An open-source framework for equations of state and classical density functional theory. *Industrial & Engineering Chemistry Research* **2023**, *62* (12), 5347-5357.

(28) Ravikovitch, P. I.; Vishnyakov, A.; Russo, R.; Neimark, A. V. Unified approach to pore size characterization of microporous carbonaceous materials from N2, Ar, and CO2 adsorption isotherms. *Langmuir* **2000**, *16* (5), 2311-2320.
(29) Yang, K.; Lin, Y.; Lu, X.; Neimark, A. V. Solvation forces between molecularly rough surfaces. *Journal of Colloid and Interface Science* **2011**, *362* (2), 382-388. DOI: https://doi.org/10.1016/j.jcis.2011.06.056.
(30) Tikhonov, A. N. On the regularization of ill-posed problems. In *Doklady Akademii Nauk*, 1963; Russian Academy of Sciences: Vol. 153, pp 49-52.

Supplementary Files

This is a list of supplementary files associated with this preprint. Click to download.

- H2asamolecularprobesubmittedSI.docx